RSC Advances

PAPER

View Article Online
View Journal | View Issue

Cite this: *RSC Adv.*, 2018, **8**, 16251

Fabrication of a superhydrophobic mesh based on PDMS/SiO_2 nanoparticles/PVDF microparticles/KH-550 by one-step dip-coating method†

Zhonglin Luo, *[abc] Yan Li,[a] Cong Duan[a] and Biaobing Wang*[ab]

Received 16th April 2018
Accepted 19th April 2018

DOI: 10.1039/c8ra03262a

rsc.li/rsc-advances

In this study, a facile one-step dip-coating approach was reported for fabrication of superhydrophobic copper mesh by using PDMS, SiO_2 nanoparticles, PVDF microparticles and a couple agent 3-aminopropyltriethoxysilane (KH-550). It is found that undesirable SiO_2 agglomeration was obviously reduced by introducing KH-550 and PVDF microparticles. The KH-550 acts as the bridge-linker and binds SiO_2, PVDF and PDMS together. The as-prepared superhydrophobic mesh exhibited a promising water contact angle of 160.1° and a small sliding angle of 2.5°. The coating displayed excellent resistance to various pollutants and retained its superhydrophobicity after abrasions (sandpaper abrasion or adhesive tape tear). The strong chemical stability was also observed when the mesh was immersed in various solutions, especially in neutral and alkaline solutions. The applications of the superhydrophobic mesh for quantitative water droplet manipulation and oil spill cleanup were also illustrated. The method is facile and economic, and could be used for large-scale fabrications for industrial applications.

1. Introduction

Wettability is an important property of solid surfaces.[1,2] A surface with a water contact angle (CA) greater than 150° and a sliding angle (SA) less than 10° is called superhydrophobic. Because of the limited contact area of the solid surface with water, superhydrophobic surfaces display various special properties, such as water repellency,[3,4] self-cleaning,[5,6] anti-icing,[7,8] anti-corrosion,[6,7] low drag for fluid flow,[9,10] and so on. Learned from nature, artificial superhydrophobic surfaces have been fabricated for applications in life and industry.[9,11–13] It was widely known that the superhydrophobic properties are the result of the combination of materials with low surface free energy and hierarchical micro- and nano-structures of the surface. The maximum achievable water contact angle is around 120° on a flat surface with a surface energy as low as 6.7 mJ m^{-2},[14] thus various technologies have to be applied to construct rough surfaces.[15,16] Most of these superhydrophobic surfaces are fabricated by complicated procedures or expensive facilities, which restrict their extensive applications. Thus it is still highly demanded to fabricate superhydrophobic surfaces with facile and low cost approaches.

Nanoparticles are promising materials used to construct roughness.[3,5,17,18] Based on solvent techniques, nanoparticles are readily introduced onto the material surfaces. In order to enhance the adhesion between the superhydrophobic coating and substrate, the bonding layer[5,17] and nanoparticle/polymer blends[19,20] have been applied. Nanoparticles always tend to agglomerate due to their high surface area and surface energy. The inter-particle forces within the agglomeration stem from the van der Waals, capillary, and electrostatic forces.[21] Nanoparticle aggregation usually form multi-scale roughness including the nano-scale roughness of primary nanoparticles and the micro-scale roughness of nanoparticle aggregates,[22] which is beneficial to form Cassie–Baxter contact state,[23] that a liquid droplet sits on the surface asperities with air pockets trapped in between, and therefore increases the water repellency. Double structured roughness was also constructed with both nano- and micro-particles recently.[3,24] These fabrications usually included complicated self-assembling techniques and multiple operation procedures. Usually, the more the nanoparticles deposit on it, the higher roughness the surface has, but the less the binding strength between nanoparticles and substrate surface becomes.[19,20] The resistance to mechanical tear and wear is a very important issue of superhydrophobic surfaces to their practical applications. Without proper design, the surface hydrophobic layers are prone to be damaged by mechanical abrasion, leading to undesired loss of water repellent properties.

[a]*School of Material Science and Engineering, National Experimental Demonstration Center for Materials Science and Engineering, Changzhou University, Changzhou, 213164, P. R. China. E-mail: zhonglinluo@cczu.edu.cn; biaobing@cczu.edu.cn*

[b]*Jiangsu Collaborative Innovation Center of Photovolatic Science and Engineering, Changzhou, Jiangsu, 213164, P. R. China*

[c]*State Key Laboratory of Molecular Engineering of Polymers, Fudan University, Shanghai, 200433, P. R. China*

† Electronic supplementary information (ESI) available. See DOI: 10.1039/c8ra03262a

Polydimethylsiloxane (PDMS) is a typical elastomeric material with a low surface energy of about 20 mJ m^{-2}. PDMS and silica (SiO_2) nanoparticles have been used to fabricate superhydrophobic surfaces on various substrates, such as metal plates,[25] woods,[26] glass,[19,22] meshes,[27,28] fabrics,[29,30] polymer films,[31] *etc.* By applying a suspension of nanoparticles in PDMS solution, superhydrophobic surfaces coated with PDMS/SiO_2 nanocomposites have been realized with facile and economic methods, such as spin coating,[32] spray coating,[19,31] dip-coating,[27,29] *etc.* Among them, dip-coating was appropriate for large scale fabrications. For the lack of strong interactions between PDMS and SiO_2 particles, serious aggregations of nanoparticles and even cracks could be observed especially at high SiO_2 contents,[19] and the durability of superhydrophobic surfaces to mechanical wear and tear was usually weak. To improve particle dispersion and increase their compatibility with polymer matrices, surface modification of particles was usually adopted.[24,30]

Polyvinylidene fluoride (PVDF) also has a low free energy. Because of its excellent heat resistance, weatherability, and chemical resistance, PVDF received extensive attentions. For the preparation of superhydrophobic surfaces, PVDF usually need to be dissolved into solvents and superhydrophobic films could be fabricated by inert solvent-induced phase-inversion techniques.[33,34] PVDF based coating techniques were also developed with the incorporation of nanoparticles.[35,36] One of the disadvantages of PVDF based coatings is that they have poor adhesion with most substrates. Therefore, pre-treatment of the surfaces is required.[35] As we know, there is no report about using commercial PVDF powder particles directly to construct superhydrophobic surfaces.

In this paper, PDMS, SiO_2 nanoparticles, and PVDF microparticles were used to construct the superhydrophobic surface on the copper mesh through a simple one-step dip-coating method. The cross-linked PDMS acts as the adhesive agent, SiO_2 nanoparticles and PVDF microparticles were adopted to construct the surface roughness. A coupling agent 3-aminopropyltriethoxysilane (KH-550) was used to improve the interactions between particles and PDMS. The prepared coatings were well characterized by using field emission scanning electron microscopy (FESEM), Fourier transform infrared spectroscopy (FTIR), X-ray photo-electron spectroscopy (XPS), and energy dispersive spectroscopy (EDS). It is found that the nanoparticle agglomeration was reduced by introducing PVDF microparticles and KH-550. The as-prepared superhydrophobic mesh displayed excellent self-cleaning properties, good resistance to acid and base attack, and desirable mechanical stability against sandpaper abrasion damage and adhesive tape tear. The applications of the coated mesh for water droplet manipulation and oil collection were also illustrated. The method is facile and economic, and is suitable for the large-scale industrial fabrications.

2. Experimental

2.1 Materials

SiO_2 (AEROSIL® R974, the density of silanols on the surface 0.39/nm^2, average diameter ≈ 12 nm (ref. 37)) was obtained from Evonik Degussa. PDMS (Sylgard® 184) was purchased from Dow Corning. PVDF (Solef® 1015) was obtained from Solvay. KH-550, toluene, magnesium sulfate, absolute ethanol, sodium hydroxide, sulfuric acid and ammonia were obtained from Sinopharm Group Chemical Reagent Co., Ltd. The adhesive tape, copper mesh (100 mesh) and sandpaper (1500 mesh) were obtained from local stores. The copper meshes were cut into rectangle (3.5 cm × 4.0 cm) pieces and rinsed with ethanol before use. Other materials were used as received.

2.2 Fabrication of hydrophobic meshes

The superhydrophobic meshes were prepared by one-step dip-coating method. For example, a typical PDMS/SiO_2/PVDF/KH-550 mesh was prepared as following. Firstly, 2.5 g PDMS (with 10% curing agent), 3.125 g SiO_2, 1.73 g PVDF and 0.433 g KH-550 (1 wt%) were added into 50 ml toluene. The solution was stirred at 80 °C for 4 hours, then stirred at room temperature for 1 h to form a homogenous paint-like suspension solution. The stirrer speed was set at 600 rpm. A piece of blank copper mesh was immersed into the above solution for 5 min, drawn out at a rate of 3 mm min^{-1}, and dried in the oven at 80 °C for 2 h.

For the sake of comparison, the PDMS/SiO_2/KH-550, PDMS/SiO_2/PVDF and PDMS/SiO_2 coated meshes were also prepared similarly to the above described process, but lack of PVDF, KH-550, or both of them in the dipping solutions respectively.

2.3 Characterization

FTIRs of the samples were analyzed in a region of 400–4000 cm^{-1} using a Nicolet Avatar 370 (Nicolet, USA). The spectra of coatings were achieved by KBr pellets and the vibrational transition frequencies are reported in wave numbers (cm^{-1}). SEM images were taken on a SUPRA55 field emission scanning electron microscope (Zeiss, Germany). The elemental maps on the coating surfaces were obtained using an EDS spectrometer (Oxford) of SEM. XPS was carried out on a Thermo Scientific™ Escalab spectrometer equipped with monochromatic Al Kα radiation (1486.6 eV) as the X-ray source (Thermo ESCALAB 250). The electron kinetic energy was recorded and converted to binding energy based on a calibration with the C1s peak (284.6 eV) and used a pass energy of 100.0 eV or 20.0 eV. Measurement of the wetting properties of the copper meshes was carried out on a video optical contact angle system (JC2000D1, Shanghai Powereach Digital Technology Equipment Co., Ltd., China) at ambient temperature. A 5 μL water droplet was used for the contact angle (CA) measurement. By adjusting the tilted angle of the sample to make a water drop (5 μL) rolling off the copper mesh, the sliding angle (SA) was obtained. CAs and SAs were determined by averaging values measured at six different points on each sample surface.

2.4 Self-cleaning test in air

Three tests were used to illustrate the self-cleaning property of the prepared PDMS/SiO_2/PVDF/KH-550 mesh. First, a water droplet (dyed by dark-blue ink) was put onto the mesh for 10 min, and tilt the mesh to remove the water droplet. Then, the mesh was put into dark-blue ink dyed water and drawn out to

test whether the mesh would be dyed by the ink. Last, green chalk powder acting as a mimic of dirt was put onto the mesh surface, water was dropped onto the surface to remove the dirt.

2.5 Coating stability test

The stability of the coatings was examined with various tests, such as chemical stability, adhesive tape tear test, and sandpaper abrasion test with repetitions. In the chemical stability test, the mesh was immersed into either acidic or alkaline solutions with different pH between 1 and 13, rinsed with distilled water and dried. The water CAs and SAs were measured in different times. The various solutions were adjusted to the desired pH values by addition of sulfuric acid or ammonia. In the adhesive tape tear test, an adhesive tape was pasted onto the mesh, pressed with the thumb and then peeled off.[38,39] This process was carried out repeatedly, and the corresponding water CAs and SAs after every five tests was recorded. To further demonstrate the good mechanical strength, the coated mesh was placed onto the 1500 mesh sandpaper and covered with a 2.5 cm × 2.8 cm glass slide. Then the mesh was dragged longitudinally and transversely (10 cm for each direction) respectively under a weight of 100 g, this process is defined as one cycle.[5] The test was repeated several times and corresponding water CAs and SAs were recorded.

3. Results and discussion

3.1 Characterization of superhydrophobic meshes

PVDF powder alone was insoluble in toluene and it was precipitated at the bottom of the bottle (Fig. S1a†). When hydrophobic SiO_2 nanoparticles were added into the solution, after agitation, a homogenous and stable paint-like suspension solution was obtained (Fig. S1b†). Because of the high specific surface area, fumed SiO_2 nanoparticles were prone to aggregate and form a suspension network in the solution, and PVDF particles would be suspended in the network.

To verify the presence of PVDF on the copper mesh, the surface components of PDMS/SiO_2 and PDMS/SiO_2/PVDF meshes were scratched down, and the FTIR spectra of the two samples as well as the pure PVDF powder were measured and shown in Fig. 1. Appearance of the peak between 3300 cm^{-1} and 3700 cm^{-1} is due to the –OH stretching vibration. The peaks at around 2964 cm^{-1}, 1261.2 cm^{-1} and 802.2 cm^{-1} are the asymmetric –CH_3 stretching, symmetric –CH_3 deformation and –CH_3 rocking in Si–CH_3 of PDMS, respectively. A broad, multi-component peak ranging from 930 cm^{-1} to 1200 cm^{-1} is corresponding to the asymmetric Si–O–Si stretching vibration absorption[25,40,41] (Fig. 1a). Compared with the PDMS/SiO_2 sample, the absorption bands at around 761.2, 615.6, 535.6, 409.8 cm^{-1}, which can be assigned to the crystal vibration absorption peaks of PVDF,[42] could be clearly seen in the spectra of the PDMS/SiO_2/PVDF sample (Fig. 1b). The weak PVDF crystal absorption peaks in the PDMS/SiO_2/PVDF sample are due to the presence of the SiO_2 nanoparticles on the surfaces of the PVDF microparticles as disclosed in the following XPS and EDS measurements. Therefore, it is reasonable to infer that the

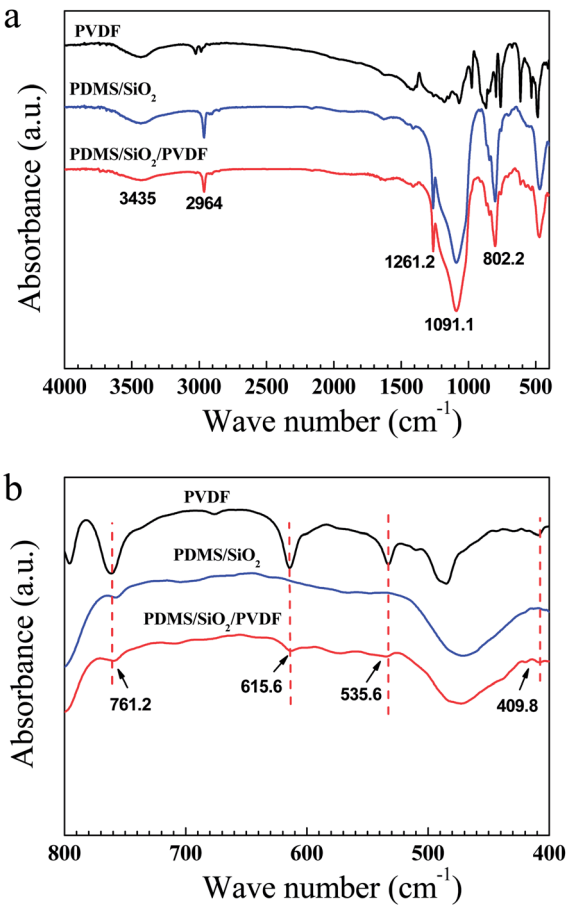

Fig. 1 FTIR spectra of PVDF powder, PDMS/SiO_2 and PDMS/SiO_2/PVDF samples.

mesh surface was effectively modified by SiO_2 nanoparticles and PVDF microparticles.

The optical images of the prepared meshes were shown in Fig. 2. The surface of the dried PDMS/SiO_2 mesh displays many tiny cracks on it (Fig. 2a). The toluene evaporation induced the internal flow during the drying process, and the cross-linked PDMS network had relatively high viscosity, thus the light nanoparticles were prone to forming aggregations and attaching onto the substrate.[22] This led to the formation of cracks on the surface, especially at high SiO_2 content.[19] When PVDF powder was added into the solution, the cracks were more obvious (Fig. 2b) because of the incompatibility of PVDF and PDMS. Fig. 2a and b also indicated that both SiO_2 and PVDF particles have weak interactions with PDMS and the copper mesh. After adding KH-550 into the dipping solution, the formed PDMS/SiO_2/KH-550 and PDMS/SiO_2/PVDF/KH-550 meshes were neat and smooth, and no cracks were found by naked eyes on the surfaces (Fig. 2c and d). Obviously, KH-550 plays an important role in improving the dispersion of SiO_2 and PVDF particles in PDMS.

When PVDF powder was added, the CA increased from 153.6° ± 3.6° of the PDMS/SiO_2 mesh to 157.8° ± 2.3° of the PDMS/SiO_2/PVDF mesh (Fig. 2a and b), and the SA slightly decreased from 3.9° ± 1.0° to 3.4° ± 1.6° correspondingly. Both

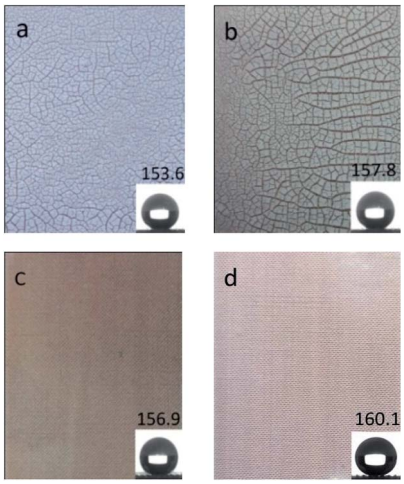

Fig. 2 Optical images of superhydrophobic meshes: (a) PDMS/SiO_2, (b) PDMS/SiO_2/PVDF, (c) PDMS/SiO_2/KH-550, and (d) PDMS/SiO_2/PVDF/KH-550. The insets are corresponding CAs, respectively.

the low surface energy of PVDF and the improved roughness contributed to it. The addition of KH-550 further optimized the superhydrophobicity of the meshes, and the CAs and SAs were $156.9° \pm 2.9°$ and $3.4° \pm 1.4°$ for the PDMS/SiO_2/KH-550 sample (Fig. 2c), and $160.1° \pm 2.1°$ and $2.5° \pm 0.6°$ for the PDMS/SiO_2/PVDF/KH-550 mesh (Fig. 2d), respectively. Thus, the uniform distribution of the particles is beneficial to form a superhydrophobic surface.

It is found that amines could form hydrogen bonds with PVDF.[43] Amines also enter into strong interactions with SiO_2 nanoparticles by three kinds of interactions (Fig. 3b): amine groups form hydrogen bonds with silanol groups (hydrogen bonding interactions), amines accept protons from isolated silanol groups (Brönsted interactions), and amines coordinate to SiO_2 nanoparticles (IV) when coordinative defect points are present on the surfaces (Lewis interactions).[37] Therefore, amine groups of KH-550 could react with SiO_2 and PVDF particles. The oxyethyl groups of KH-550, on the other end, would be hydrolyzed by absorbing water vapour in air, and the formed silanol groups could react with the hydroxyl groups of PDMS or form hydrogen bonds to PVDF. Therefore, KH-550 acts as the bridge-linker to bind SiO_2 nanoparticles, PVDF microparticles and PDMS. The multiple interactions among them were shown in Fig. 3a as a schematic chemical reaction process. The increased interactions among SiO_2, PVDF and PDMS led to the formation of well-distributions of particles on the sample surfaces.

The SEM images of PDMS/SiO_2/KH-550 and PDMS/SiO_2/PVDF/KH-550 meshes were shown in Fig. 4. Compared with the surface of the PDMS/SiO_2/KH-550 mesh, granular bulges with the diameters from 1 to 15 μm could be clearly seen on the PDMS/SiO_2/PVDF/KH-550 mesh (Fig. 4c), which indicated the PVDF microparticles were successfully coated on the mesh surface. The agglomerations of SiO_2 nanoparticles were obviously seen on the surface of PDMS/SiO_2/KH-550 mesh in the high magnification SEM image (Fig. 4b), while nanoparticles were distributed more homogenously on the surface of the PDMS/SiO_2/PVDF/KH-550 mesh (Fig. 4d). These results indicated the microparticles, because of the much larger sizes and weights, would further prevent nanoparticles from forming agglomerations. The EDS elemental maps showed the uniform distribution of C, O and Si on the surface of PDMS/SiO_2/PVDF/KH-550 mesh (Fig. 5), while F was only observed on PVDF microparticles (Fig. 5, S2 and Table S1†). Because of the low content of KH-550, the N element was not detected by the EDS measurement. The Si element was also found on the surface of PVDF particles (Fig. S2†), which indicates SiO_2 adsorbed on the surfaces of PVDF microparticles.

XPS studies were further carried out to get the chemical compositions of the outmost layers (Fig. 6 and Table 1). The C1s (285 eV), O1s (532 eV), Si2s (155 eV) and Si2p (103 eV) peaks can be seen clearly in the spectra of all samples. After introduction of PVDF, KH-550, or both of them, however, no clear peaks associated with the F and N elements could be found in the spectra. The elemental XPS spectra for F and N were further measured by using a pass energy of 20 eV (Fig. S3†). Only a very small F1s peak around 688 eV was observed in PDMS/SiO_2/PVDF, and almost no fluorine element could be detected on the surface of PDMS/SiO_2/PVDF/KH-550 mesh (Fig. S3a†). The results indicated the SiO_2 nanoparticles and PDMS covered the surface of PVDF microparticles during the drying process. Also, a very weak N1s peak at 400 eV, which is attributed to nitrogen moieties with covalent N–H bonds in KH-550, could be seen in PDMS/SiO_2/KH-550 and PDMS/SiO_2/PVDF/KH-550 samples (Fig. S3b†). The weak intensity is because of the low contents of KH-550 in them. Also, SiO_2 nanoparticles and PDMS are prone

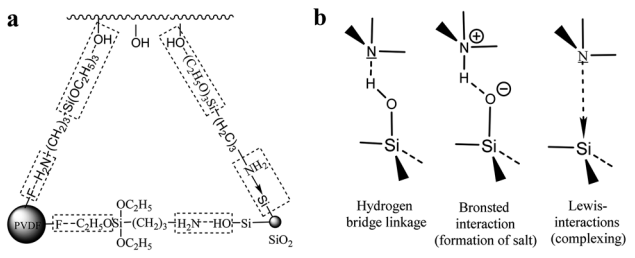

Fig. 3 (a) The KH-550 acts as the bridge-linker to bind SiO_2, PVDF and PDMS. (b) Possible interactions between an amine and the surface of SiO_2 nanoparticles.[37]

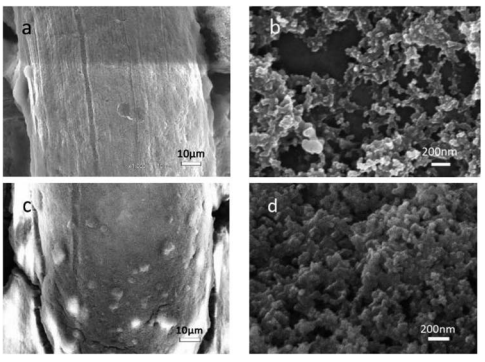

Fig. 4 SEM images of the coated surface. (a) and (b) are PDMS/SiO_2/KH-550 mesh, (c) and (d) are PDMS/SiO_2/PVDF/KH-550 mesh at different magnifications.

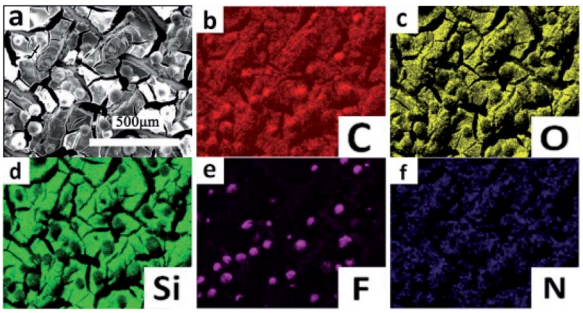

Fig. 5 (a) SEM image and (b–f) EDS C, O, Si, F and N elemental maps of the PDMS/SiO_2/PVDF/KH-550 mesh.

to moving to the surfaces to decrease the surface energy of the coatings, which further reduce the contents of N elements on the surfaces. After adding KH-550, the content of C element increases and that of the O element decreases (Table 1), indicating that PDMS migrated to the coating surfaces. Therefore, the interaction between PDMS and particles became stronger.

The PDMS/SiO_2/PVDF/KH-550 mesh was chosen for further studies due to its outstanding superhydrophobicity. The optical images of water droplets (dyed by dark-blue ink) and oil droplets (dyed by Sudan red) on the pristine copper mesh and the superhydrophobic mesh were shown in Fig. 7a. Because of the porous structure, the pristine copper mesh is hydrophobic and has a CA around 120°. In comparison, the water droplet almost keeps a spherical shape on the surface of the modified mesh. The CA of oil droplet on the surface of the pristine mesh is small, while the oil droplet quickly spreads on the modified mesh, indicating the PDMS/SiO_2/PVDF/KH-550 mesh is superoleophilic. A jet of water easily bounces off the superhydrophobic mesh due to the trapped air between the water and mesh (Fig. 7b and Movie S1†). Moreover, the superhydrophobic mesh appears bright silver with a mirror-like phenomenon when it was pressed into water, further proving the air cushion between water and the superhydrophobic mesh (Fig. 7d).

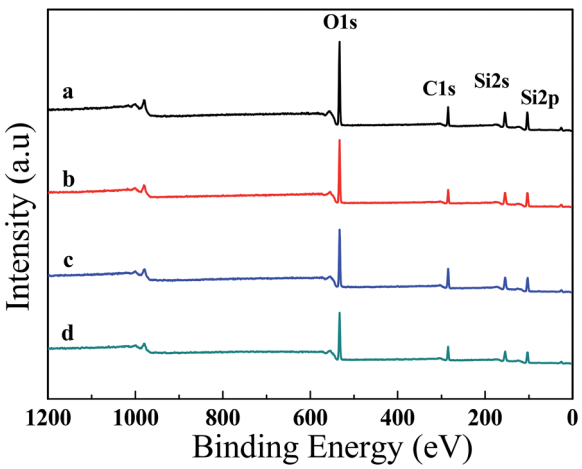

Fig. 6 XPS survey spectra of (a) PDMS/SiO_2, (b) PDMS/SiO_2/PVDF, (c) PDMS/SiO_2/KH-550 and (d) PDMS/SiO_2/PVDF/KH-550 mesh.

Table 1 Elemental compositions of different superhydrophobic meshes

	Compositions (at%)				
Mesh	C	Si	O	N	F
PDMS/SiO_2	23.97	32.41	43.62	—	—
PDMS/SiO_2/PVDF	21.59	35.77	42.42	—	0.22
PDMS/SiO_2/KH550	32.2	30.96	36.11	0.73	—
PDMS/SiO_2/PVDF/KH550	28.11	31.6	39.5	0.47	0.31

3.2 Self-cleaning properties of superhydrophobic meshes

The coated mesh also exhibited excellent antifouling and self-cleaning properties. When a water droplet (dyed by dark-blue ink) was put onto the coated mesh for 10 min and then removed by tilting the mesh, no stain was found on it (Fig. 8(a and b) and Movie S2†). When the mesh was immersed into ink dyed water and lifted up, no water droplets were adhered on the surface (Fig. 7(c and d) and Movie S3†). Moreover, the model contaminant was also easily cleared away from the coated mesh by dropping water (Fig. 7(e and f) and Movie S4†). These excellent self-cleaning properties were due to the air cushion between the solid and liquid interface.

3.3 Stability of superhydrophobic meshes

The stability of the coating in long term contact with water should be taken into consideration for outdoor products. Therefore, the PDMS/SiO_2/PVDF/KH-550 meshes were immersed in various solutions with different pH values, and the water CAs and SAs were measured to assess the chemical stability of the superhydrophobic meshes. As shown in Fig. 9, CAs gradually decreased when the meshes were immersed in all solutions. In neutral solution, the CA became 151.4° after 8

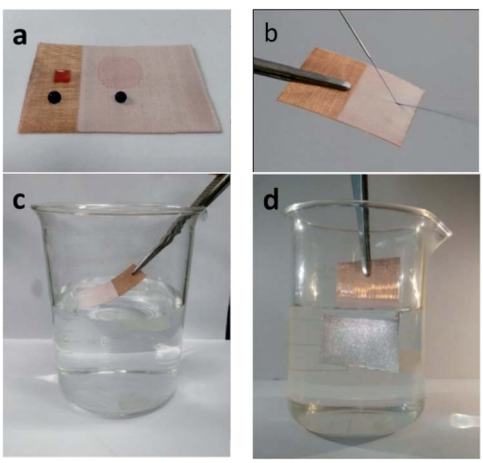

Fig. 7 (a) Optical images of water droplets (dyed by blue-black ink) and *n*-hexane droplets (dyed by Sudan red) on the surfaces of the pristine and coated mesh. (b) A jet of water bounces off the coated mesh. (c) The coated mesh is immersed in water by an external force. (d) The immersed mesh appears bright silver due to the existence of trapped air.

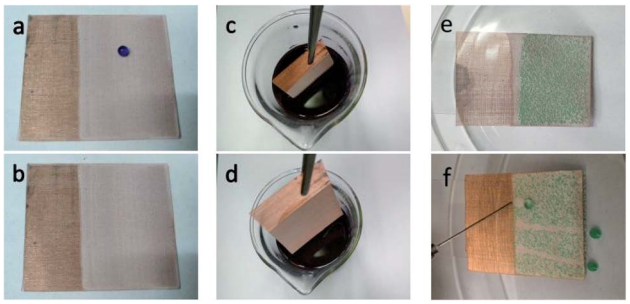

Fig. 8 (a) and (b) A water droplet (dyed by dark-blue ink) was put onto the coated mesh for 10 min, and then removed. (c) and (d) The mesh was inserted into dark-blue ink dyed water and lifted up. (e) and (f) The model contaminant (green chalk dust) was easily cleared away from the mesh.

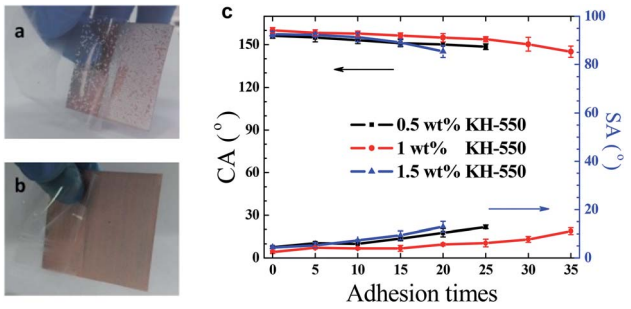

Fig. 10 An adhesive tape peeled off (a) from PDMS/SiO_2 mesh after the first time tear test and (b) from PDMS/SiO_2/PVDF/KH-550 mesh after 35 times of tear tests, (c) water CAs and SAs of PDMS/SiO_2/PVDF/KH-550 mesh after repeated tear tests.

days, and with the increase of the immersion time to 10 days, the CA decreased to 145.7°. The decrease of CAs was a little more obvious in acidic or alkaline solutions.

The variations of SAs along with different pH levels are also illustrated in Fig. 9. The SA increased with the immersion time, and the water droplets could roll off the coatings if the meshes were in neutral or alkaline solutions for 8 days. After 10 day immersion, the droplets were stuck on the coatings occasionally, which means the transition from the Cassie–Baxter state to the Wenzel state.[38] It was reported that the variation of hydrophobic performance after the water immersion is attributed to a weakening of the Si–CH_3 bond strength.[3] The results indicated the meshes have good resistance to neutral and alkaline aqueous solutions.

For acidic treatments, though the CAs decreased gradually, the SAs were more sensitive to the damage of superhydrophobic surfaces.[38,44] The droplets became adhesive to the meshes when they were immersed in the solutions of pH 5, 3, 1 for more than 6, 4 and 3 days, respectively. This is because the acid would attack the amine groups and the multiple interactions among SiO_2, PVDF and PMDS were gradually eliminated. Acid also reacted with the exposed copper wires. Consequently, a portion of the nanostructured area started to get damaged, resulting in increasing SAs. Such results indicated that the mesh has medium-good stability against acidic solutions.

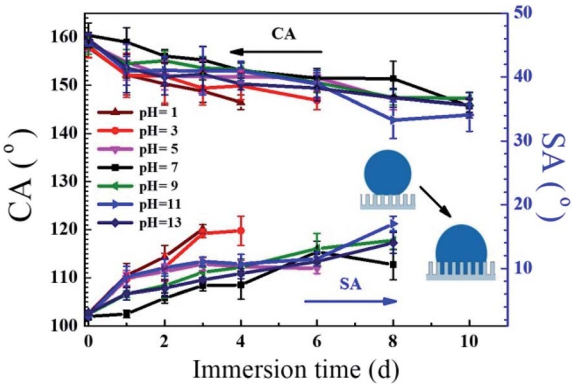

Fig. 9 The CAs and SAs as a function of immersion time in pH solutions (pH = 1–13).

The mechanical stability of the coating was assessed by the repeated tear tests with adhesive tapes.[38,39] In this test, an adhesive tape was pasted onto the coated mesh, pressed with thumb, and then peeled off.[39] As shown in Fig. 10a, the PDMS/SiO_2 coating was easily peeled off, demonstrating the coating stability was poor. In comparison, CAs and SAs changed slowly with the increase of the tear cycles. After repetition for 35 cycles, the PDMS/SiO_2/PVDF/KH-550 mesh remained superhydrophobic and the water droplets rolled off the tilted coating successfully (Fig. 10b and c). Thus the PDMS/SiO_2/PVDF/KH-550 coating is firmly attached to the copper mesh. The results implied that KH-550 improved the adhesion strength of the coatings. The effect of KH-550 content on the adhesion strength was also tested. When KH-550 is 0.5 wt%, adhesion strength of the prepared mesh is less than that containing 1 wt% KH-550. This result is because of the less bonding strength between particles and PDMS matrix. When KH-550 is 1.5 wt%, the decreased tear stability may be caused by the more PDMS on the coating surface, which would reduce the roughness of the surface. The increased KH-550 content would induce more –NH_2 groups on the surface, which also decreased the superhydrophobicity of the surface.

The sandpaper abrasion tests[5,39] were also carried out on the PDMS/SiO_2/PVDF/KH-550 mesh. The mesh weighing 100 g was placed face-down to sandpaper (1500 meshes) and moved transversely and longitudinally for 10 cm respectively along the guided line as shown in Fig. 11a–d. This process is defined as one abrasion cycle. The water CAs and SAs after every five abrasion cycles are shown in Fig. 11e. When 1 wt% KH-550 was contained, the water CA decreased gradually to 151.6° and SA became larger than 10° after 30 cycles. But water droplets still could roll off the 14° tilted mesh after 35 cycles, which means that the water droplets are also in the Cassie–Baxter state. Therefore, the mesh has robust resistance to mechanical abrasions. The KH-550 content also influences the abrasion mechanical properties of the meshes, which was consistent with the results in the above tear test.

Surface modification of particles was often adopted to improve particle dispersion and increase their compatibility with polymer matrix. Recently, PDMS-coated silica nanoparticles prepared by a thermal vapor deposition method were

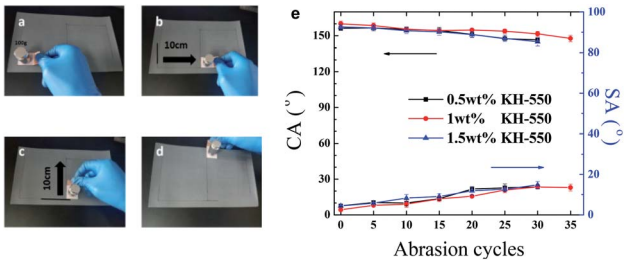

Fig. 11 Sandpaper abrasion tests. (a–d) One cycle of the sandpaper abrasion test. (e) Water CAs and SAs of PDMS/SiO_2/PVDF/KH-550 mesh after repeated abrasion tests.

used to provide a superhydrophobic characteristic to fabrics and meshes.[28] The prepared PDMS-coated SiO_2/PDMS steel mesh showed negligible changes of CAs when it was exposed to acidic and basic environments for 40 min. And the superhydrophobic property was maintained when the mesh was impacted by 100 g of sands with velocity about 0.22 m s^{-1}. In comparison, more strong tolerance to chemical corrosions was observed in this study and excellent mechanical stability was also exhibited. The results is due to the multiple bridge-link interactions provided by the KH-550 couple agent. In a recent experimental report, improved mechanical properties and good adhesion of the PVDF/SiO_2 composites coating on the glass substrate were also found when the substrate was pre-treated with KH-550 molecules.[35] It was also reported that the additional cross-linking points provided by silane agents could improve the mechanical properties of superhydrophobic coatings considerably.[38] These results are consistent well with our findings. The hydrophobic SiO_2 nanoparticles, PVDF powder, PDMS and KH-550 were all commercially available and inexpensive, therefore can be utilized in real industrial applications.

3.4 The application of superhydrophobic mesh

3.4.1 Water droplet manipulation. Based on the superhydrophobic mesh, we designed a device that uses negative pressure for the transfer of microdroplets (Fig. 12a and S4†). As shown in Fig. 12b, without the assistant of negative pressure, a 5 μL water droplet can not be transferred on the superhydrophobic mesh. When a negative pressure (about 0.8 kPa) was applied to the back of the mesh, an obvious deformation of the droplet was observed when the syringe needle was slowly receded. Then the droplet was separated from the needle and successfully transferred onto the superhydrophobic mesh (Fig. 12c). With this droplet capture device and a quantitative syringe needle, we can rapidly prepare the micro/nanoliter droplets with controllable volumes ranging from 0.3 to 5 μL (Fig. 12d). Therefore the micro/nanoliter droplet could be manipulated by giving or repealing the negative pressure.

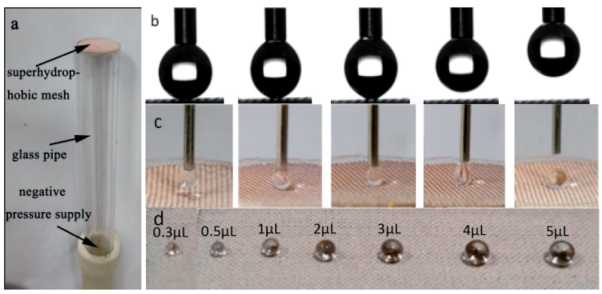

Fig. 12 (a) Illustration of the microdroplet capture device. (b) A droplet of 5 μL water can not be transferred on the superhydrophobic mesh without the assistant of negative pressure. (c) A droplet of 5 μL water was successfully transferred onto the superhydrophobic mesh with the assistant of negative pressure. (d) With the droplet capture device and a quantitative syringe needle, the micro/nanoliter droplets with controllable volumes ranging from 0.3 to 5 μL could be rapidly prepared.

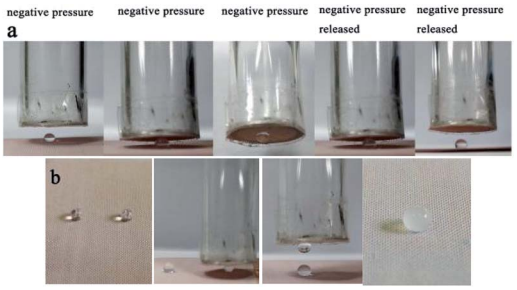

Fig. 13 (a) A 5 μL droplet can be transferred conveniently by changing the negative pressure. (b) Microdroplet-based microreactions can be achieved easily with the device.

With the above device, microdroplet-based microreactions can be achieved conveniently (Fig. 13). A drop of 5 μL magnesium sulfate (1 M) and a drop of 5 μL sodium hydroxide (2 M) were transported to the superhydrophobic mesh, then the drop of magnesium sulfate was grabbed and put to the sodium hydroxide droplet, the white precipitate of magnesium hydroxide occurred later (Fig. 13b), demonstrating the potential strategy for the quantitative microdroplets reaction.

3.4.2 Oil collection. The porous structure and superoleophilicity of the mesh surface ensure the infiltration of oils through the mesh, and superhydrophobic mesh have exhibited promising applications in oil spills cleanup.[10] We also tested the capability of the prepared mesh for oil collection. As shown in

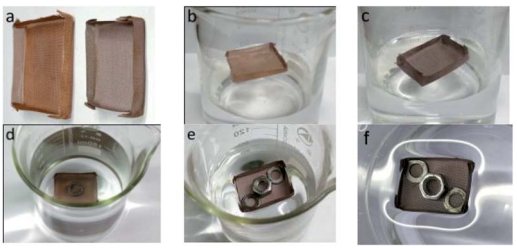

Fig. 14 (a) Mini boats fabricated from the pristine mesh and superhydrophobic mesh. Both the pristine mesh boat (b) and superhydrophobic mesh boat (c) floating freely on water. (d) The pristine mesh boat cannot load weight and sink after a day. (e) The superhydrophobic mesh boat can load weight (2.71 g) and float on water for five days. (f) Overhead view of the superhydrophobic mesh boat with load floating on water.

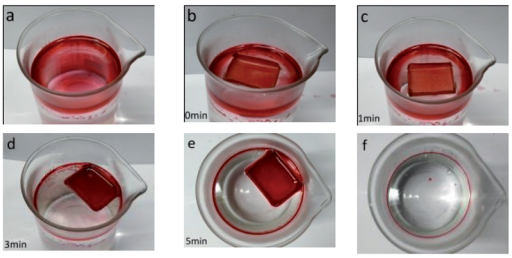

Fig. 15 The *in situ* collection of an oil spill by a superhydrophobic mesh boat.

Fig. 14, two mini boats with a size of 2.8 cm × 2 cm × 0.5 cm were fabricated from the pristine mesh and superhydrophobic mesh. Without loading, both of the two boats could float freely on water (Fig. 14b and c). However, the pristine mesh boat sunk after one day when a load of 0.39 g was added (Fig. 14d), while the superhydrophobic mini boat still float freely on water after five days and could hold a load of ~4 times of the boat weight (the weight of boat and loading are 0.67 and 2.71 g, respectively; Fig. 14e). As shown in Fig. 14f, there is an air cushion beneath the boat, and the deformation of the water surface occurs under the mini boat, yielding a force to support the weight of the boat and loads.

To demonstrate the ability of oil spill cleanup, xylene dyed with red oil (2.0 g) was used as a model oil spill, and the superhydrophobic mesh boat was put on the oil spill. As shown in Fig. 15, the oil permeated and entered into the boat, and after 5 min, almost all the oil was automatically collected by the mini boat. During the whole process, no external force was needed. About 1.83 g of xylene was collected, which includes 0.17 g xylene absorbed by the mesh and 1.66 g xylene in the boat. The oil recovery was approximated as 91.5%. The collection process is self-driven, and no additional energy is required, displaying an energy-saving and efficient application for oil collection. And if a vacuum pump could be equipped with the boat, the collection could be continuous, unmanned and highly efficient.

4. Conclusions

In summary, we provide a facile one-step dip-coating method to prepare a durable superhydrophobic mesh based on PDMS, SiO_2 nanoparticles and PVDF microparticles. Different from surface treatment of nanoparticles and microparticles, a coupling agent KH-550 was added to act as the bridge-linker to bind PDMS, SiO_2 and PVDF. The method could be applied to other organic polymers and inorganic spheres. The prepared mesh exhibited well dispersion of nanoparticles and microparticles in PDMS matrix, excellent superhydrophobicity, self-cleaning properties, adhesion resistance and wear resistance. Also, good stability was observed after immersion in different aqueous solutions. Furthermore, the probable applications of the superhydrophobic meshes in precise microdroplet-based reaction and oil spill cleanup were also illustrated.

Conflicts of interest

There are no conflicts to declare.

Acknowledgements

Financial support from the Natural Science Foundation of China (Grant No. 21304012), the Natural Science Foundation of Jiangsu Province (BK20130249), the Top-notch Academic Programs Project of Jiangsu Higher Education Institutions (TAPP), the Priority Academic Program Development of Jiangsu Higher Education Institutions (PAPD), and State Key Laboratory of Molecular Engineering of Polymers (Fudan University, K2018-06) is gratefully acknowledged.

References

1 T. Sun, L. Feng, X. Gao and L. Jiang, *Acc. Chem. Res.*, 2005, **38**, 644–652.
2 S. Nishimoto and B. Bhushan, *RSC Adv.*, 2013, **3**, 671–690.
3 G. Momen and M. Farzaneh, *Appl. Surf. Sci.*, 2012, **258**, 5723–5728.
4 J. Marchalot, S. M. M. Ramos, C. Pirat and C. Journet, *Appl. Surf. Sci.*, 2018, **428**, 364–369.
5 Y. Lu, S. Sathasivam, J. Song, C. R. Crick, C. J. Carmalt and I. P. Parkin, *Science*, 2015, **347**, 1132–1135.
6 S. S. Latthe, P. Sudhagar, A. Devadoss, A. M. Kumar, S. Liu, C. Terashima, K. Nakata and A. Fujishima, *J. Mater. Chem. A*, 2015, **3**, 14263–14271.
7 N. Wang, D. Xiong, Y. Deng, Y. Shi and K. Wang, *ACS Appl. Mater. Interfaces*, 2015, **7**, 6260–6272.
8 L. Wang, Q. Gong, S. Zhan, L. Jiang and Y. Zheng, *Adv. Mater.*, 2016, **28**, 7729–7735.
9 M. J. Zhai, Y. F. Gong, X. Y. Chen, T. H. Xiao, G. P. Zhang, L. H. Xu and H. Li, *Surf. Coat. Technol.*, 2017, **328**, 115–120.
10 G. Wang, Z. Zeng, H. Wang, L. Zhang, X. Sun, Y. He, L. Li, X. Wu, T. Ren and Q. Xue, *ACS Appl. Mater. Interfaces*, 2015, **7**, 26184–26194.
11 W. Yu, J. Tao, X. Yu, S. Zhao, S. T. Tu and H. Liu, *Appl. Energy*, 2017, **185**, 1233–1244.
12 C. Li, R. Guo, X. Jiang, S. Hu, L. Li, X. Cao, H. Yang, Y. Song, Y. Ma and L. Jiang, *Adv. Mater.*, 2009, **21**, 4254–4258.
13 B. Su, S. Wang, Y. Song and L. Jiang, *Nano Res.*, 2011, **4**, 266–273.
14 T. Nishino, M. Meguro, K. Nakamae, M. Matsushita and Y. Ueda, *Langmuir*, 1999, **15**, 4321–4323.
15 X. M. Li, D. Reinhoudt and M. Crego-Calama, *Chem. Soc. Rev.*, 2007, **36**, 1350–1368.
16 S. Wang, K. Liu, X. Yao and L. Jiang, *Chem. Rev.*, 2015, **115**, 8230–8293.
17 M. Liu, J. Li, Y. Hou and Z. Guo, *ACS Nano*, 2017, **11**, 1113–1119.
18 H. Chen, X. Zhang, P. Zhang and Z. Zhang, *Appl. Surf. Sci.*, 2012, **261**, 628–632.
19 K. Li, X. Zeng, H. Li, X. Lai, C. Ye and H. Xie, *Appl. Surf. Sci.*, 2013, **279**, 458–463.

20 C. Cai, N. Sang, S. Teng, Z. Shen, J. Guo, X. Zhao and Z. Guo, *Surf. Coat. Technol.*, 2016, **307**, 366–373.
21 Y. Raichman, M. Kazakevich, E. Rabkin and Y. Tsur, *Adv. Mater.*, 2006, **18**, 2028–2030.
22 N. Gao, Y. Y. Yan, X. Y. Chen and D. J. Mee, *Mater. Lett.*, 2011, **65**, 2902–2905.
23 A. B. D. Cassie and S. Baxter, *Trans. Faraday Soc.*, 1944, **40**, 546–551.
24 Q. Ke, W. Fu, H. Jin, L. Zhang, T. Tang and J. Zhang, *Surf. Coat. Technol.*, 2011, **205**, 4910–4914.
25 S. Deniz and B. Arikan, *Int. J. Eng. Appl. Sci.*, 2016, **8**, 19–27.
26 H. Chang, K. Tu, X. Wang and J. Liu, *RSC Adv.*, 2015, **5**, 30647–30653.
27 D. Guo, J. Xiao, J. Chen, Y. Liu, C. Yu, M. Cao and L. Jiang, *Small*, 2015, **11**, 4491–4496.
28 E. J. Park, B. R. Kim, D. K. Park, S. W. Han, D. H. Kim, W. S. Yun and Y. D. Kim, *RSC Adv.*, 2015, **5**, 40595–40602.
29 C. H. Xue, M. Li, X. J. Guo, X. Li, Q. F. An and S. T. Jia, *Surf. Coat. Technol.*, 2017, **310**, 134–142.
30 S. W. Han, E. J. Park, M.-G. Jeong, I. H. Kim, H. O. Seo, J. H. Kim, K.-D. Kim and Y. D. Kim, *Appl. Surf. Sci.*, 2017, **400**, 405–412.
31 J. Wang, H. Chen, X. Wang and Z. Q. Yuan, *Appl. Phys. A: Mater. Sci. Process.*, 2016, **122**, 968.
32 Z. He, M. Ma, X. Lan, F. Chen, K. Wang, H. Deng, Q. Zhang and Q. Fu, *Soft Matter*, 2011, **7**, 6435–6443.
33 W. B. Zhang, Z. Shi, F. Zhang, X. Liu, J. Jin and L. Jiang, *Adv. Mater.*, 2013, **25**, 2071–2076.
34 C. H. Xue, X. Li, S. T. Jia, X. Guo and M. Li, *RSC Adv.*, 2016, **6**, 84887–84892.
35 D. Kumar, L. Li and Z. Chen, *Prog. Org. Coat.*, 2016, **101**, 385–390.
36 T. Liu, X. Li, D. Wang, Q. Huang, Z. Liu, N. Li and C. Xiao, *Appl. Surf. Sci.*, 2017, **396**, 1443–1449.
37 R. Bode, H. Ferch and H. Fratzscher, in *Technical Bulletin Fine Particles*, Degussa AG, Frankfurt/M., 2006, vol. 11, pp. 1–72.
38 B. Li and J. Zhang, *Chem. Commun.*, 2016, **52**, 2744–2747.
39 A. K. Singh and J. K. Singh, *RSC Adv.*, 2016, **6**, 103632–103640.
40 K. Berean, J. Z. Ou, M. Nour, K. Latham, C. McSweeney, D. Paull, A. Halim, S. Kentish, C. M. Doherty, A. J. Hill and K. Kalantar-zadeh, *Sep. Purif. Technol.*, 2014, **122**, 96–104.
41 K. Efimenko, W. E. Wallace and J. Genzer, *J. Colloid Interface Sci.*, 2002, **254**, 306–315.
42 R. Gregorio, *J. Appl. Polym. Sci.*, 2006, **100**, 3272–3279.
43 Z.-M. Dang, H.-Y. Wang and H.-P. Xu, *Appl. Phys. Lett.*, 2006, **89**, 112902.
44 B. Li and J. Zhang, *Carbon*, 2015, **93**, 648–658.